NEGATIVE TRIANGULARITY SCENARIOS: FROM TCV AND AUG EXPERIMENTS TO DTT PREDICTIONS

A. MARIANI, P. MANTICA, I. CASIRAGHI
Institute for Plasma Science and Technology, CNR
Milano, Italy
Email: alberto.mariani@istp.cnr.it

L. AUCONE, D. BRIOSCHI
Dipartimento di Fisica 'G. Occhialini', Università di Milano-Bicocca
Milano, Italy

A. BALESTRI, F. BAGNATO, J. BALL, S. CODA, O. SAUTER, M. VALLAR
École Polytechnique Fédérale de Lausanne (EPFL), Swiss Plasma Center (SPC)
Lausanne, Switzerland

G. MERLO
Oden Institute for Computational Engineering and Sciences, University of Texas at Austin,
Austin, USA

R. AMBROSINO
Università degli Studi di Napoli Federico II
Napoli, Italy

T. BOLZONELLA, P. INNOCENTE, P. MUSCENTE, N. VIANELLO
Consorzio RFX (CNR, ENEA, INFN, Università di Padova, Acciaierie Venete SpA)
Padova, Italy

L. BALBINOT
Università della Tuscia, Dipartimento di Economia, Ingegneria, Società e Impresa (DEIM)
Viterbo, Italy

A. CASTALDO, V. FUSCO, G. VLAD
ENEA C.R.Frascati,
Frascati, Italy

L. FRASSINETTI
Fusion Plasma Physics, ECSS, KTH Royal Institute of Technology
Stockholm, Sweden

T. HAPPEL, J. HOBIRK, R.M. MCDERMOTT, T. PÜTTERICH, F. SCIORTINO, C.F.B. ZIMMERMANN
Max-Planck-Institut für Plasmaphysik
Garching, Germany

B. VANOVAC
Plasma Science and Fusion Center, Massachusetts Institute of Technology
Cambridge, USA

THE EUROFUSION TOKAMAK EXPLOITATION TEAM[1], TCV TEAM[2], ASDEX UPGRADE TEAM[3]

Abstract

Experiments, gyrokinetic simulations and transport predictions have been performed to investigate if a negative triangularity (NT) L-mode option for the DTT full power scenario would perform similarly to the positive triangularity (PT) H-mode reference scenario, avoiding the harmful edge localized modes (ELMs). The simulations show that if a beneficial effect of NT would not come from the edge-SOL region $\rho_{tor} > 0.9$, one should renounce to part of the PT H-mode performance to avoid the ELMs. New dedicated experiments at TCV and AUG, with similar shapes and transport regimes, show that even with the small triangularity of the considered DTT scenarios, a beneficial effect of NT could come from $\rho_{tor} > 0.9$, allowing NT L-modes to overperform corresponding PT L-modes, reaching central pressures comparable to larger power PT H-modes. For AUG, a similar central plasma performance is found with PT and NT for a PT/NT ELMy H-mode/H-mode couple of pulses and for a PT/NT non-ELMy H-mode/L-mode one, both with ECRH only. The beneficial effect of NT was

[1] See the author list of "Progress on an exhaust solution for a reactor using EUROfusion multi-machines capabilities" by E. Joffrin et al. to be published in Nuclear Fusion Special Issue: Overview and Summary Papers from the 29th Fusion Energy Conference (London, UK, 16-21 October 2023).

[2] See H. Reimerdes et al 2022 Nucl. Fusion 62 042018 (https://doi.org/10.1088/1741-4326/ac369b).

[3] See Stroth et al. 2022 Nucl. Fusion 62 042006 (https://doi.org/10.1088/1741-4326/ac207f).

shown by gyrokinetic runs to be due to an increase of the critical temperature logarithmic gradient when inverting the triangularity, with similar stiffness for positive and negative triangularity. The effect has been found in both ITG- and TEM-dominant micro-instability regimes.

1. INTRODUCTION

Experiments performed at TCV [1], DIII-D [2] and AUG [3] indicate that it is possible, in some cases, for L-mode plasmas featuring negative triangularity (NT) [4], i.e. plasmas with D-shape convexity directed towards the inside of the torus instead of the outside, to perform comparably to H-mode plasmas with standard 'D-shaped' cross-section (positive triangularity: PT). In NT plasmas, a H-mode-like plasma performance can be achieved avoiding the detrimental edge localized modes (ELMs) that could potentially damage the tokamak in fusion reactor regimes [5, 6]. Since the physics behind the performance improvement in NT compared to PT is not yet fully understood, current experimental, theoretical, and numerical analysis is ongoing in order to investigate it. This is required for extrapolating to possible future NT fusion reactors.

A NT option is under investigation for the full power scenario of the Divertor Tokamak Test (DTT) facility [7]. DTT is under construction in Italy and aims to test alternative designs and materials for the divertor, within the roadmap to the DEMO. Since DTT is still under construction, two different approaches were followed by the authors to investigate the predicted performance of the DTT NT scenario: first, a numerical modelling effort by means of predictive transport simulations and gyrokinetic simulations of the DTT scenario has been performed [8,9], then dedicated experiments at TCV [10,11] and AUG [12] were carried out under EUROfusion WP TE 2022 campaign, obtaining plasmas with NT shape close to the DTT one with similar turbulent transport regimes. The outcome of this analysis is collected here, comparing the results that have been obtained with the numerical and experimental approaches, in order to construct a coherent picture of the underlying physics.

The numerical analysis of the DTT scenario has been carried out as follows: predictive simulations with the transport code ASTRA [13], coupled with the quasilinear model TGLF SAT2 [14], have been run at first. The PT H-mode reference DTT full power scenario with neon seeding has been compared with the NT L-mode option, calculating self-consistently the NBI/ECRH/ICRH power input and the impurity profiles. Then, these results have been validated at two selected radii by gyrokinetic simulations, made with the GENE code [15].

In TCV experiments, in addition to the PT H-mode/NT L-mode comparisons, PT L-modes have been obtained, to understand how the transport in L-mode improves when changing the sign of the triangularity from PT to NT. Moreover, different proportions of NBI and ECRH heating have been applied, namely NBI only, mixed NBI/ECRH and ECRH only, to access different turbulent regimes. When NBI injection was present, PT/NT L-modes with lower NBI power have been compared with PT H-modes with double NBI power. The results have then been confronted with ASTRA-TGLF SAT2 transport simulations, and GENE at selected radii.

Unlike TCV plasmas, NT discharges in AUG tend to go into H-mode at lower input power when operated with the ion ∇B drift pointing towards the X-point (called 'favorable configuration'). Thus, both 'favorable' and 'unfavorable' configurations have been obtained, to include in the PT/NT comparisons at least one discharge operating in L-mode. The PT discharges at AUG were not made within NT scope. They were compared with the NT pulses since they were performed at high shaping and comparable q (same current and field). The experiments have been interpreted with ASTRA-TGLF SAT2 simulations. The gyrokinetic analysis of AUG pulses is ongoing.

2. DTT/TCV/AUG PREDICTIVE TRANSPORT MODELLING AND TCV/AUG EXPERIMENTAL RESULTS

The DTT full power scenario with Ne seeding is being designed by means of integrated modelling [16,17]. The effect of changing the triangularity from positive to negative on the plasma performance has been investigated by our group by running numerical simulations, and by carrying out experiments with similar shapes and transport properties on the TCV and AUG tokamaks, as described in the introduction. The plasma shapes of the PT/NT DTT full power scenarios, as well as the main geometrical parameters of interest for the analysis, such as the safety factor q, the triangularity δ and the elongation κ, are shown in Fig.1 in black. Here, $\rho_{tor} = \sqrt{\phi/\phi_{edge}}$ is the normalized toroidal radius, where ϕ is the flux of the toroidal magnetic field. A selection of corresponding quantities from TCV and AUG experiments are shown in red and blue, respectively. As can be observed in Fig.1, the DTT shapes and triangularities have been reproduced with a good approximation in TCV and AUG

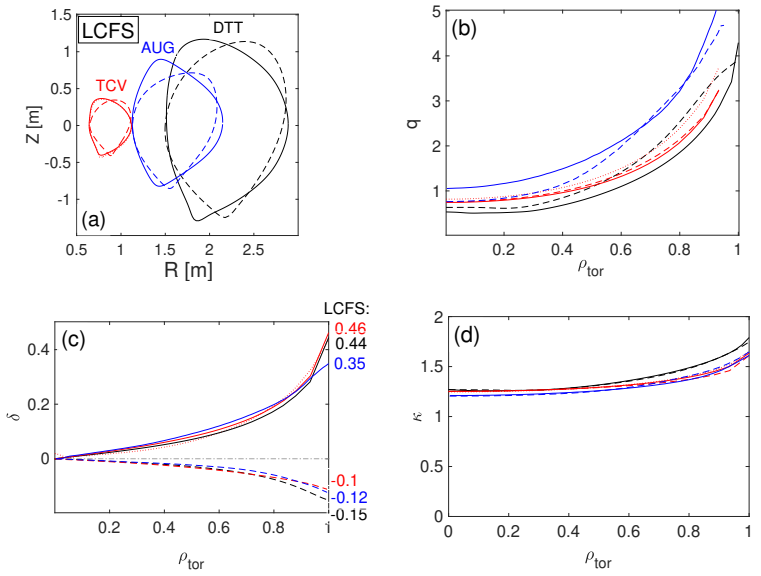
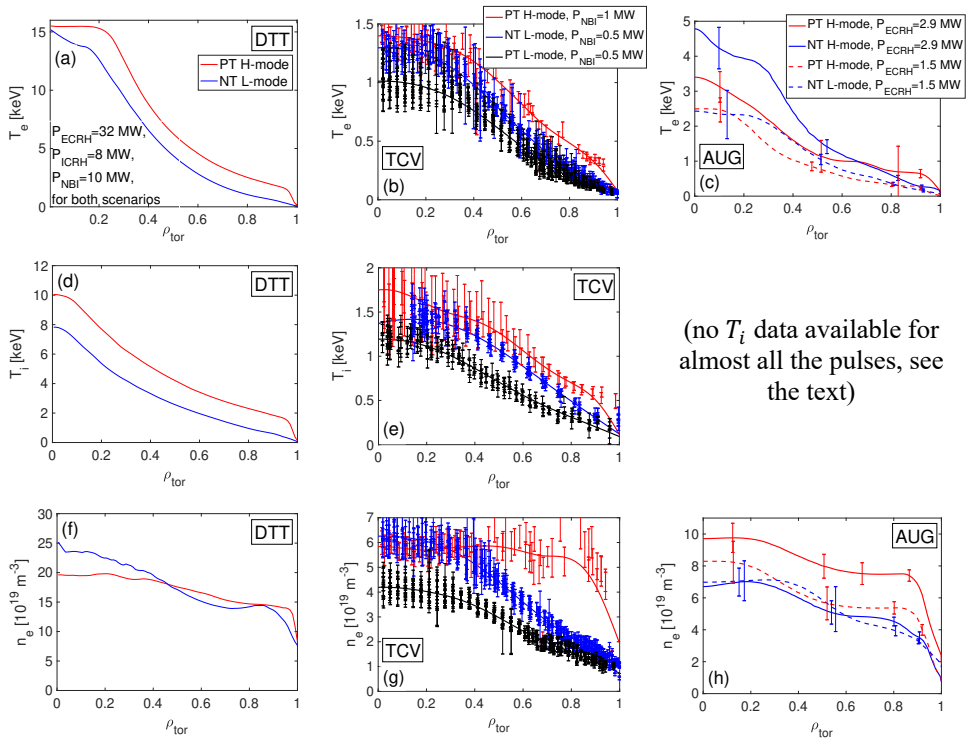


FIG.1. (a) Plasma shapes (last close flux surface: LCFS) for DTT PT/NT scenarios (black solid/dashed), TCV pulses #73392/#73388/#73382 (PT H-mode/PT L-mode/NT L-mod, red solid/dotted/dashed) and AUG pulses #36157/#40473 (PT/NT H-modes, blue solid/dashed). (b), (c), (d) safety factor q, triangularity δ and elongation κ radial profiles, corresponding to the cases in (a), following the same color/line-style codes.

experiments. The elongation has been reduced in TCV and AUG pulses, compared with the DTT reference profiles, to avoid vertical displacement events (VDEs), as can be seen in Fig.1 (d). For DTT, the LCFS shapes were computed with the free boundary CREATE-NL solver [18] and the equilibria inside the LCFS with ASTRA using the SPIDER equilibrium code [19]. The TCV experimental equilibria are obtained with LIUQE [20], while the AUG equilibria with IDE [21].

The DTT ASTRA-TGLF predictive transport simulations, performed with density and temperature boundary conditions at $\rho_{tor} = 0.94$, show that the NT L-mode scenario is not able to recover the loss of the PT H-mode pedestal and reach similar central n, T values. This is shown in the first column of Fig.2, where T_e, T_i and n_e are shown for the PT (red) and NT (blue) scenarios. Fig.2 shows the same cases of Fig.1, for clarity. Moreover, ASTRA-TGLF shows for these DTT cases that only flipping the triangularity of the last close flux surface (LCFS) does not impact the predicted profiles [8]. TGLF stand-alone finally indicates that the triangularity of the NT scenario should be approximately 9 times larger than the reference one to allow T_i to recover the loss of the PT H-mode pedestal for $\rho_{tor} > 0.7$, where the triangularity is sufficiently large to matter.



(no T_i data available for almost all the pulses, see the text)

FIG. 2. DTT (first column): ASTRA-TGLF predicted profiles: PT reference H-mode full power scenario with neon seeding and corresponding NT L-mode scenario, both with injected P_{ECRH}=32 MW, P_{ICRH}=8 MW, P_{NBI}=10 MW; TCV (second column): experimental profiles: comparison of higher NBI power PT H-mode (#73392, t=0.72s-0.74s, P_{NBI}=1 MW) with half power PT/NT L-modes (#73388/#73382, both for t=0.68s-0.79s). AUG (third column): experimental profiles: PT/NT H-modes with P_{ECRH}=2.9 MW (#36157, t=4.6s-4.9s/#40473, t=3s-3.5s), PT/NT H/L-modes (#40647, t=3.4s-4s/#40866, t=2.6s-2.8s). (a,d,f) are adapted from [8], (b,e,g) from [10,11], while (c,h) from [12].

The TCV experiments, surprisingly, draw a completely different picture. An example is shown in the second column of Fig.2, corresponding to cases with only NBI: a larger NBI power PT H-mode (red) is compared with half power PT(black)/NT(blue) L-modes. Fig.2

shows that the NT L-mode performs significantly better than the PT L-mode, reaching central T_e, T_i and n_e comparable to the PT H-mode, which has double injected NBI power. This is exactly how one would wish the NT to behave, differently from what was predicted by the DTT simulations of [8]. A similar picture has also been obtained for mixed ECRH/NBI pulses or ECRH only ones (for ECRH only pulses only a PT/NT L-mode couple was obtained).

The AUG picture is more complicated. Let us start from the comparison of two PT/NT ELMy H-modes with ECRH only (same ECRH power). This is shown in the third column of Fig.2 by red/blue solid lines (the ion temperature has not been shown for consistency, since it has only been measured for pulse #40473 at the considered time slice). The NT discharge presents a smaller pedestal, but it recovers the PT T_e values for $\rho_{tor} >$ 0.8, reaching ~40% larger central values. However, the NT central density is ~30% smaller than the PT one, resulting in similar electron pressure. The picture is also similar for a H-mode/L-mode PT/NT couple that has been obtained performing the L-mode in the 'unfavorable configuration', which results are shown in the third column of Fig.2 by dashed lines. Here, the NT L-mode recovers the central T_e of the PT H-mode, with a slightly smaller central density, thus obtaining a similar electron pressure. However, in this case the PT plasma is an ELM-free H-mode (EDA) [22, 23], therefore there is no practical gain for this case when changing the triangularity to NT, since in both pulses there are no ELMs.

To estimate the change in plasma confinement properties when changing the triangularity, it is useful to introduce 0D parameters such as the energy confinement time τ_E= (plasma stored energy/rate of energy loss) and the normalized beta $\beta_N = \beta\,(aB_T/I_P)$, where $\beta =$ (kinetic pressure/magnetic pressure), $a =$ minor radius, $B_T =$ toroidal magnetic field and $I_P =$ plasma current. These are shown for the main TCV and AUG

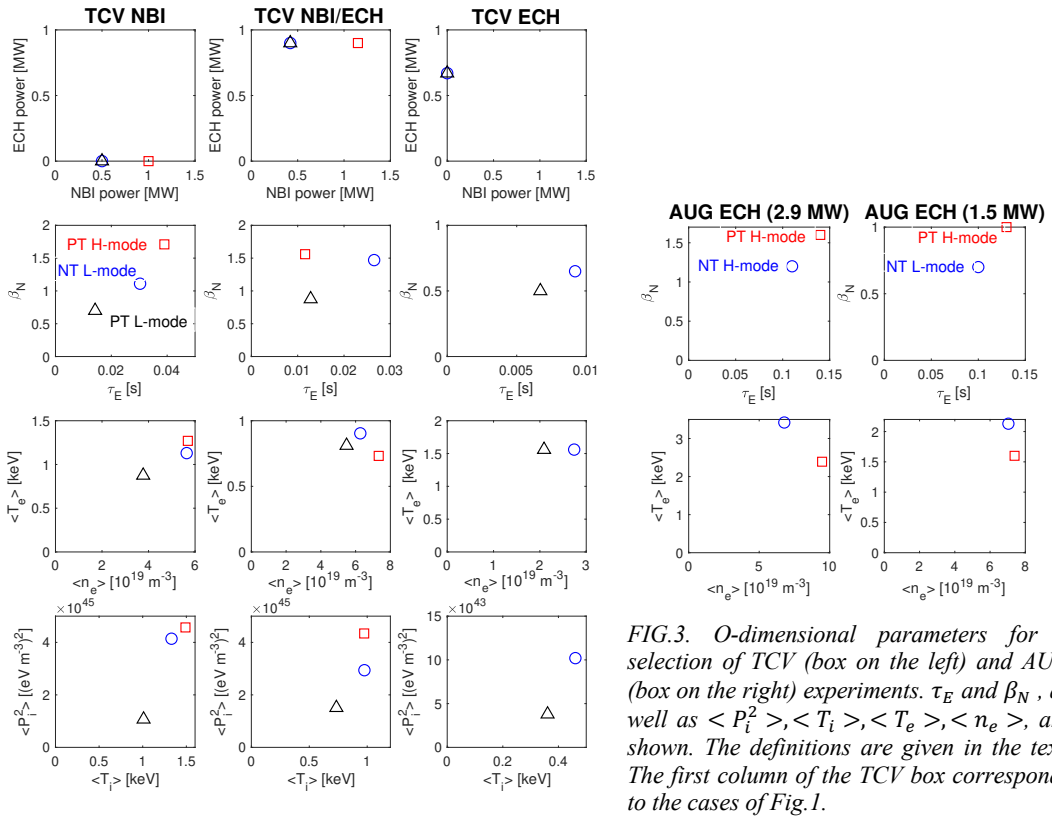


FIG.3. O-dimensional parameters for a selection of TCV (box on the left) and AUG (box on the right) experiments. τ_E and β_N , as well as $< P_i^2 >, < T_i >, < T_e >, < n_e >$, are shown. The definitions are given in the text. The first column of the TCV box corresponds to the cases of Fig.1.

experiments in Fig.3. The TCV experiments with mixed ECRH/NBI and ECRH only, which were excluded in the previous figures for brevity, are also shown here. One notes that the TCV NT L-modes (blue circles) perform better (have larger τ_E and β_N) than the corresponding PT L-modes (black triangles), positioning themselves between the PT L-modes and the higher power PT H-modes for the NBI only case (for the mixed ECRH/NBI pulses, a MHD mode deteriorates the performance of the H-mode). For AUG cases, the PT H-modes perform better than both the NT H- and L- modes. However, one can better specify what 'better performance' means. Since the fusion gain is proportional to P_i^2 and the fusion neutrons are mainly produced in the inner core, a better fusion performance is obtained when larger pressures/temperatures are reached in the plasma central region. Therefore, the average values of n, T at the plasma center are more meaningful than τ_E and β_N, which are global quantities, computed over the entire plasma volume, giving large weight to the plasma

edge, which does not produce fusion neutrons. Thus, the volume averages of P_i^2, T_e, T_i and n_e have been added to Fig.3. They are computed as: $< A >= \frac{1}{V}\int_0^{0.4} d\rho_{tor} \frac{dV}{d\rho_{tor}} A(\rho_{tor})$, where $A = P_i^2$, T_e, T_i, n_e and V is the volume enclosed by the $\rho_{tor} = 0.4$ magnetic surface, since this is the key region for the fusion production. For TCV cases, the NT L-modes have always larger $< P_i^2 >, < T_i >, < T_e >, < n_e >$ than the PT L-modes (except for $< T_e >$ in the ECRH only case, which is the same for NT L-mode/PT L-mode). Moreover, the NT L-modes have intermediate $< P_i^2 >$ between lower power PT L-modes and larger power PT H-modes, almost reaching the double power PT H-mode in the NBI only case. For AUG, even though the PT H-mode has larger τ_E and β_N than the NT H-mode, the NT H-mode has larger $< T_e >$ (and similar $< P_e >$), which is more important for the fusion performance.

To investigate the role that the transport inside the separatrix has on the effect of the NT, one can look at the n, T logarithmic gradients. Let us consider for brevity only the T_e logarithmic gradient $a/L_{T_e} = -d\,(\log T_e)/\,d\rho_{tor}$, since T_e is measured in both TCV and AUG and the picture is similar for a/L_{T_i} (for TCV) and a/L_{n_e}. The T_e logarithmic gradients are shown in Fig.4 for the same cases of Fig.2 and Fig.1. One notes that, when comparing PT H-modes with NT L-modes, a/L_{T_e} is always larger for the H-mode outside the pedestal top, while it is smaller inside it, due to the presence of the pedestal in the H-mode, for DTT, TCV and AUG. However, when looking to TCV (Fig. 4 (b)), where also a PT L-mode is present, one notes that the NT L-mode, with the same NBI power input, develops an intermediate T_e peaking between the PT L-mode and PT H-mode, and this improvement with respect to the PT L-mode is restricted to $\rho_{tor} > 0.9$. For AUG (Fig. 4 (c)), conversely, the NT H-mode develops a larger peaking compared with the corresponding PT H-mode inside the

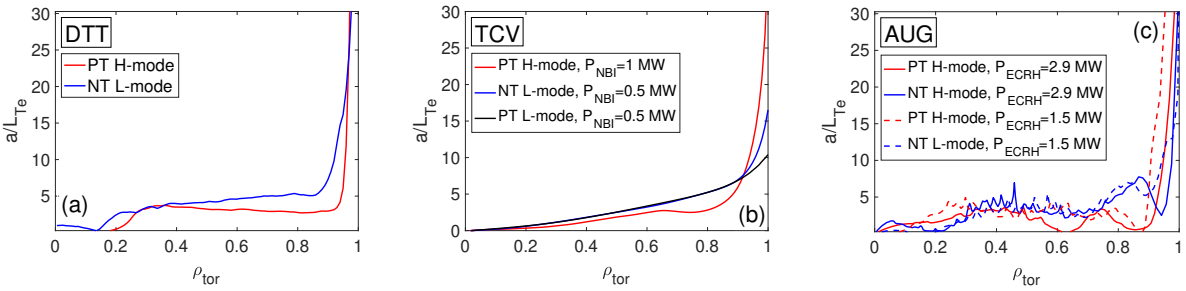


FIG. 4. Logarithmic gradients of the electron temperature profiles, corresponding to the cases of Fig.1/2. (a) DTT (ASTRA-TGLF); (b) TCV NBI only cases (exp.); (c) AUG ECRH only cases (exp.). (a)/(b)/(c) adapted from [8]/[10]/[12].

pedestal, from $\rho_{tor} > 0.7$. These results suggest that, for the considered cases, when comparing PT/NT L-modes, the NT beneficial effect comes from a reduced transport in the edge region $\rho_{tor} > 0.9$ while, when comparing PT/NT H-modes, the beneficial effect starts more inside. In particular, the effect of the n, T boundary conditions at the LCFS has been studied. For example, for TCV the impact of changing n, T at $\rho_{tor} = 1$ on the corresponding central values has been roughly evaluated by integrating the n, T profiles of the PT L-mode for $\rho_{tor} < 1$, keeping fixed the PT L-mode logarithmic gradients but taking the n, T values at $\rho_{tor} = 1$ from the corresponding NT L-mode (and vice-versa). It is found that the difference of n, T at the LCFS roughly contributes half of the difference between the central values between PT and NT L-modes, as it is shown for T_e in Fig.5 (a). The additional half comes from the improved logarithmic gradients in NT. This suggest that the physics of the SOL can contribute part of the beneficial effect of NT. This is confirmed for TCV, where steeper n, T profiles are found for NT L-modes than for PT L-modes in the SOL (corresponding to a narrower λ_q, in agreement with what was reported in [24, 25]). The overall picture agrees with what is emerging within the working group of the EUROfusion TSVV task 2, where NT L-modes are found to produce an intermediate 'proto-pedestal' between the PT H-mode pedestal and the L-mode edge,

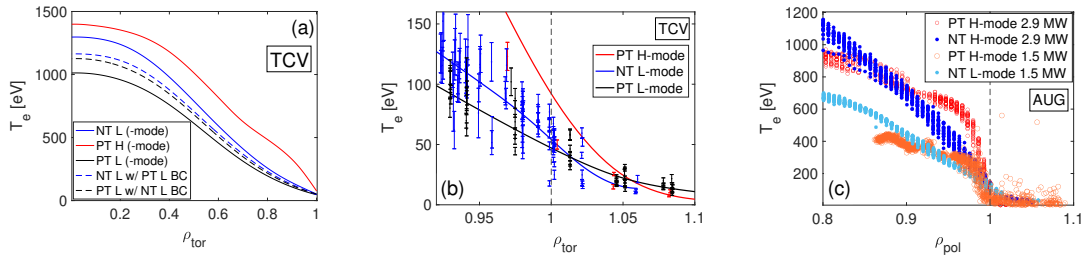


FIG. 5. (a) effect of keeping fixed the logarithmic gradients and changing the T_e value at the separatrix. (b) and (c) Experimental T_e profiles in the edge and SOL, for TCV and AUG, respectively. (a)/(b)/(c) adapted from [8]/[8]/[10].

probably due to a reduced turbulent transport around the separatrix. For AUG, even though n, T are similar for PT/NT at the LCFS, the NT cases do not present a typical H-mode pedestal, while this is compensated by larger gradients at the LCFS (unfortunately for AUG PT L-modes were not obtained, to compare with).

ASTRA-TGLF (SAT2) predictive simulations were made for TCV and AUG to reproduce the experiments. The results for the TCV cases with NBI only and AUG cases with ECRH only and higher power are shown in Fig.6.

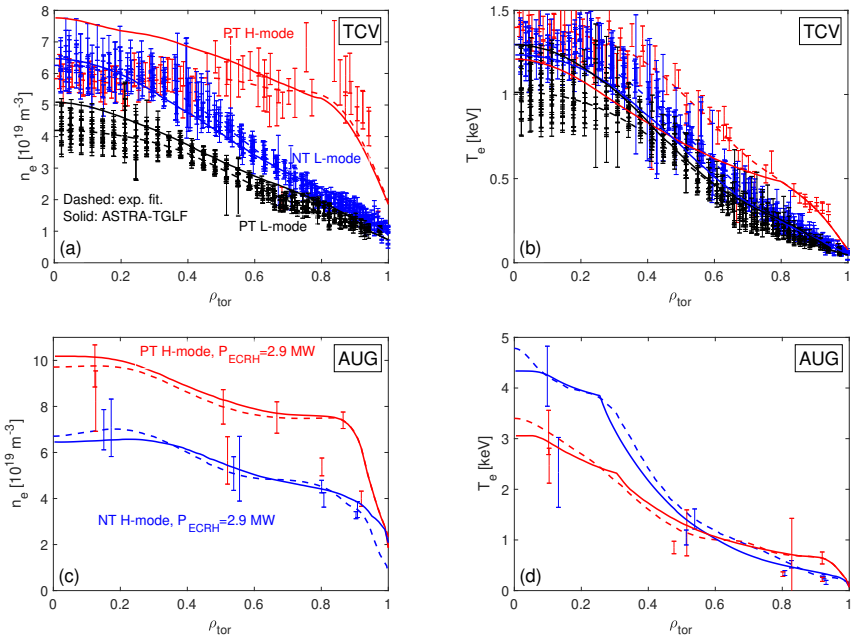


FIG. 6. ASTRA-TGLF SAT 2 predicted electron density and temperature profiles, for TCV (a)/(b) and AUG (b)/(c), compared with the experiments, for a selection from the cases of Fig.2. (a)/(b) adapted from [10], (c)/(d) adapted from [12].

For TCV, ASTRA-TGLF, with boundary conditions (BC) at $\rho_{tor} = 0.95$, is only able to reproduce n_e for the L-modes, while it fails to reproduce all the profiles in the H-mode, also when setting BC at $\rho_{tor} = 0.8$, and the temperatures for the L-modes. On the contrary, for AUG the ASTRA-TGLF runs with BC at $\rho_{tor} = 1$ for the L-mode and at the top of the pedestal for the H-modes are in good agreement with the experiment, even though TGLF underestimates the experimental a/L_{T_e} in the region $0.7 < \rho_{tor} < 0.9$. For all DTT, TCV, AUG cases, a numerical experiment has been performed, by switching the LCFS shape from NT to PT, keeping fixed the other input. For all the cases, the effect of only flipping the shape was found negligible. As a caveat, TGLF averages out the top and bottom δ to feed it to its Miller analytical equilibrium. This way, it strongly reduces the negative δ of the NT DTT scenario, which presents top negative δ in conjunction with small positive bottom δ. Thus, the effect of reversing the δ could be partially lost with this procedure in ASTRA-TGLF.

3. GYROKINETIC SIMULATIONS

Linear and nonlinear flux-tube gyrokinetic simulations have been performed with the GENE code at fixed radii for DTT and TCV, while some preliminary runs are ongoing for AUG, to validate the ASTRA-TGLF runs and/or interpret the experiments. Let us first consider the linear results. For DTT, linear scans in the poloidal wavenumber have been carried out at two radii, $\rho_{tor} = 0.7, 0.85$, where δ was supposed sufficiently large to impact the transport. For each radius, two additional shapes were considered, in addition to the PT and NT ones, obtained by rigidly flipping the LCFS with respect to the cylinder identified by the major radius R_0, and then recomputing the equilibrium inside it with CHEASE. These numerical shapes are called NT-flipped, obtained by flipping PT, and PT-flipped, obtained by flipping NT. The GENE runs have been performed including kinetic electrons, electromagnetic effects, collisions (Landau operator) and impurities (DTT: Ne and W, TCV: C). The micro-instability regime is found ITG-dominant at

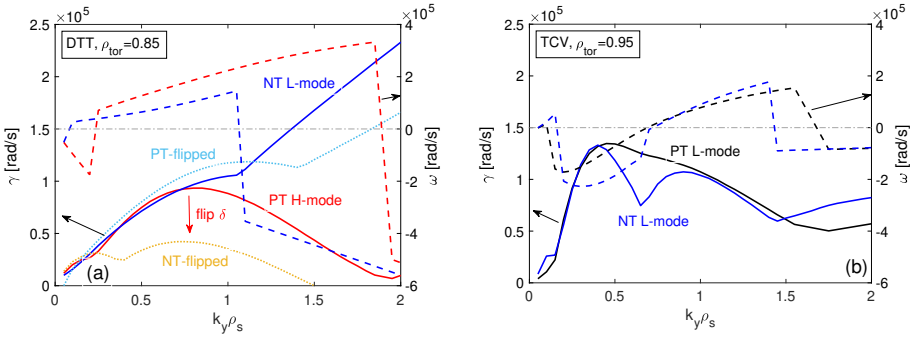


FIG. 7. Linear eigenvalues (growth rate and frequency: solid and dashed lines, respectively) of the main unstable mode, computed with GENE, for the DTT scenarios at $\rho_{tor} = 0.85$ (a) and for the TCV NBI only PT/NT L-modes at $\rho_{tor} = 0.95$ (b). (a)/(b) adapted from [6]/[8].

both radii, and a strong stabilizing effect, that halves the growth rates, is found when flipping the triangularity in H-mode from PT to NT-flipped, while a negligible effect of flipping δ is found in the L-mode, as can be seen in Fig.7 (a). For TCV, a TEM-dominant micro-instability regime is found at $\rho_{tor} = 0.85$ for the mixed ECRH/NBI and pure ECRH cases, while for the NBI only case a continuous TEM-ITG branch is found at $\rho_{tor} = 0.8$ and $\rho_{tor} = 0.95$, with only TEMs contributing the fluxes at the larger radius. The spectra of the PT/NT L-modes from the NBI only case at $\rho_{tor} = 0.95$ are shown as an example in Fig.7 (b). The impact of flipping the shape alone has been directly investigated in TCV with nonlinear simulation, as will be shown in the following.

Nonlinear GENE simulations have been performed for DTT and TCV, to estimate the effect of the negative triangularity on the heat transport. The ion temperature stiffness, i.e. the degree to which the radial T_i profile responds to changes in the applied heat fluxes, has been studied for DTT scenarios at $\rho_{tor} = 0.85$, given that the micro-instability regime was found to be ITG-dominant with the linear analysis. The results are summarized in Fig.8 (a), where GENE scans of the ion heat flux q_i versus a/L_{T_i} are shown for the four considered shapes, compared with TGLF stand-alone and with ASTRA-TGLF. An effect of flipping δ alone is only found for the H-modes, where a +36% increase of a/L_{T_i} is obtained when going from PT to NT-flipped, while the effect is negligible for the L-modes, consistently with the linear analysis. The agreement of GENE with TGLF and ASTRA-TGLF is good at the ASTRA-TGLF flux level, therefore the predictive transport analysis is validated by GENE at the radius of analysis. The NL fluxes are reduced by -61% in H-mode when flipping δ, even more than the linear stabilizing effect on the growth rates. For TCV, a strong stabilization of NT is observed in both ECRH only and NBI only cases [10], which are both TEM dominant at the radius of analysis, showing that this effect is independent of the micro-instability regime (ITG dominant for DTT cases, TEM dominant for TCV ones). The electron temperature stiffness is investigated for the case of Fig.7 (b), i.e., the PT/NT L-modes with NBI only, considering four shapes as for DTT. Here, differently from DTT shapes, NT-flipped and PT-flipped indicate the cases that are obtained from PT and NT scenarios keeping fixed the plasma profiles and switching the shapes, instead of rigidly mirroring them with respect to R_0. The T_e stiffness is investigated instead of the T_i one, since, as shown in Fig.7 (b), the turbulence is TEM driven, and the TEM main drive is a/L_{T_e}. For this case, the results are shown in Fig.8 (b) and, in contrast with what was observed in TCV L-modes, show a direct effect of the triangularity on the electron heat transport. Indeed, inverting the triangularity leads to a +30% increase of a/L_{T_e} , even larger than the +10% experimental value, with PT profiles, while an even larger effect is predicted with NT profiles. However, also a +10% gain in a/L_{T_e} is within the GENE error bars. The simulations are still running, collecting additional statistics to reduce the numerical error bars. Simulations are ongoing to understand which are the key parameters that explain the larger effect of NT in TCV or in DTT H-modes. The collisionality, which was at first identified as a key parameter, seems to be ruled out by a new GENE collisionality scan. Impurities have still to be included in this collisionality scan, thus for the moment the possibility for the collisionality to play a role is still open.

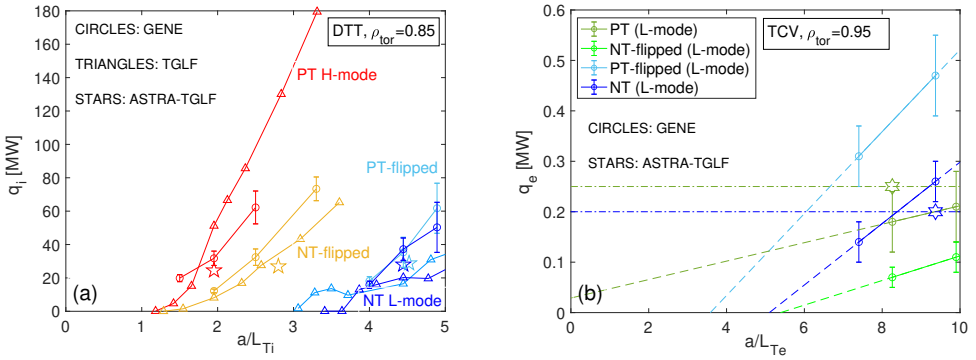


FIG. 8. Temperature stiffness for DTT at $\rho_{tor} = 0.85$ (a) and for TCV NBI only L-modes at $\rho_{tor} = 0.95$(b), corresponding to the cases of Fig.7: GENE nonlinear heat flux scans versus temperature logarithmic gradient. (a)/(b) adapted from [8]/[10].

4. CONCLUSION

- ASTRA-TGLF transport simulations with BC at $\rho_{tor} = 0.95$ predict that in the negative triangularity (NT) L-mode DTT full power scenario the $|\delta|$ value is too small to allow density and temperature profiles to overcome the loss of the PT H-mode pedestal and reach similar central values: this picture is confirmed by GENE simulations up to $\rho_{tor} = 0.85$.
- TCV experiments (similar shapes and transport conditions as in DTT): large beneficial effect of NT for different power mixes (ECRH, ECRH/NBI and NBI), with NT L-modes that overperform corresponding PT L-modes and reach central pressures similar to PT H-modes with twice the power.

- This could seem in contrast with the DTT numerical analysis, however the effect of changing the sign of triangularity on TCV experiments is limited to the edge-SOL region $\rho_{tor} > 0.9$, therefore this effect could simply have been missed in the DTT simulations: some additional effect could come from $\rho_{tor} > 0.95$, outside the ASTRA-TGLF BCs, and/or TGLF could miss part of the effect of the NT since it uses an up-down symmetric Miller equilibrium.
- AUG experiments tend to go into H-mode even with NT shapes (only one L-mode plasma was obtained): similar pressures between PT and NT pulses, but with no practical gain, since either H-mode/H-mode ELMy PT/NT pairs or H-mode non-ELMy /L-mode pairs are obtained. For the PT/NT H-mode pairs the NT effect is more inside than for TCV L-modes, in the region $0.7 < \rho_{tor} < 0.9$.
- GENE linear (DTT): strong linear and nonlinear stabilizing effects of NT on heat fluxes in both ITG- and TEM-dominant cases (DTT H-mode and TCV, respectively). This is due to a larger critical gradient for $\delta < 0$, while the temperature stiffness is similar for $\delta > 0$ and $\delta < 0$.
- GENE nonlinear (DTT): only predicts a beneficial direct effect of flipping δ on a/L_{T_i} for the H-mode at the larger considered radius $\rho_{tor} = 0.85$, while the effect is found negligible for the L-mode.
- GENE linear/nonlinear (TCV): predicts, for the NBI-only TEM-dominant case at $\rho_{tor} = 0.95$, a direct effect of switching from PT to NT shape on a/L_{T_e} for the L-modes, possibly contributing to explain the larger temperature peaking that is observed for NT compared to PT in the plasma edge region $\rho_{tor} > 0.9$, which allows the NT L-mode to reach central pressures similar to the double power PT H-mode.
- Summing up, the DTT simulations and the TCV/AUG experiments indicate that a possible beneficial effect of inverting the triangularity of the DTT full power scenario could come from the plasma edge-SOL, allowing the NT scenario to achieve central n, T values comparable to the reference PT H-mode, staying in L-mode and thus avoiding ELMs. Simulations of the edge-SOL of TCV/AUG and DTT are needed to confirm this picture, which are ongoing.

ACKNOWLEDGEMENTS

This work has been carried out within the framework of the EUROfusion Consortium, partially funded by the European Union via the Euratom Research and Training Programme (Grant Agreement No 101052200 — EUROfusion). The Swiss contribution to this work has been funded by the Swiss State Secretariat for Education, Research and Innovation (SERI). Views and opinions expressed are however those of the author(s) only and do not necessarily reflect those of the European Union, the European Commission or SERI. Neither the European Union nor the European Commission nor SERI can be held responsible for them. We acknowledge the CINECA award under the ISCRA initiative and the EUROfusion WP-AC, for the availability of high-performance computing resources and support. This work was performed within the TSVV-02 EUROfusion task. Figures 2, 4-8 are adapted from [8], [10], [12].

REFERENCES

[1] CODA, S. et al., Plasma Phys. Control. Fusion **64**, (2022) 014004.
[2] AUSTIN, M.E. et al., Phys. Rev. Lett. **122** (2019), 115001.
[3] HAPPEL, T. et al., Nucl. Fusion **63** (2023), 016002.
[4] MARINONI, A. et al., Rev. Mod. Plasma Phys **5** (2021), 6.
[5] LOARTE, A. et al., Nucl. Fusion **54** (2014), 033007.
[6] EICH, T. et al., Nucl. Mater. Energy **12** (2017), 84-90.
[7] AMBROSINO, R. et al., Fusion Eng. Des. **167** (2021), 112330.
[8] MARIANI, A. et al., submitted to Nuclear Fusion (2023).
[9] MARIANI, A. et al., poster at 48th EPS Conference on Plasma Physics.
[10] BALESTRI, A. et al., to be submitted.
[11] BALESTRI, A. et al., poster at 27th Joint EU-US Transport Task Force Meeting.
[12] AUCONE, L. et al., to be submitted.
[13] PEREVERZEV, G.V. et al., IPP Report 5/98 (2002).
[14] STAEBLER, G.M. et al., Plasma Phys. Control. Fusion **63 (**2021) 015013.
[15] JENKO, F. et al., Phys. Plasmas **7** (2000) 1904.
[16] CASIRAGHI, I. et al., Nucl. Fusion **61** (2021), 116068.
[17] CASIRAGHI, I. et al., Plasma Phys. Control. Fusion **65** (2023), 035017.
[18] ALBANESE, R. et al., Fusion Eng. Des. **96-97** (2015), 664-7.
[19] IVANOV, A.A. 2005 32nd EPS Conf. on Plasma Physics—Terragona 29C (ECA) P-5.063.
[20] MORET, J.-M. et al., Fusion Eng. Des. **91** (2015), 1.
[21] FISCHER, R. et al., 2013 40th EPS Conf. on Plasma Physics—Espoo, Finland, P-2.139
[22] VANOVAC, B. et al., EPJ Web of Conferences **277** (2023), 03003.
[23] GIL, L. et al., Nucl. Fusion **60** (2020), 054003.
[24] MUSCENTE, P. et al., poster contribution to the 49th European Conference on Plasma Physics (EPS 2023).
[25] LIM, K. et al., Plasma Phys. Control. Fusion **65** (2023), 085006.